Raman enhanced four-wave mixing in silicon core fibers

SHIYU SUN[1], MENG HUANG[1], DONG WU[1], LI SHEN[2], HAONAN REN[1], THOMAS W. HAWKINS[3], JOHN BALLATO[3], URSULA J. GIBSON[3], GORAN Z. MASHANOVICH[1], AND ANNA C.PEACOCK[1]

[1] *Optoelectronics Research Centre, University of Southampton, Southampton SO17 1BJ, UK*
[2] *Wuhan National Laboratory for Optoelectronics and School of Optical and Electrical Information, Huazhong University of Science and Technology, Wuhan 430074, China*
[3] *Center for Optical Materials Science and Engineering Technologies and Department of Materials Science and Engineering, Clemson University, Clemson, South Carolina 29634, USA*
[*] *Corresponding author: S.Sun@soton.ac.uk and acp@orc.soton.ac.uk*

Compiled December 20, 2021

A strong Raman enhancement to the four-wave mixing (FWM) conversion efficiency is obtained in a silicon core fiber (SCF) when pumped with a continuous-wave (CW) source in the telecom band. By tapering the SCFs to alter the core diameter and length, the role of phase-matching on the conversion enhancement is investigated, with a maximum Raman enhancement of $\sim 15\,\mathrm{dB}$ obtained for a SCF with a zero dispersion wavelength close to the pump. Simulations show that by optimising the tapered waist diameter to overlap the FWM phase-matching with the peak Raman gain, it is possible to obtain large Raman enhanced FWM conversion efficiencies of up to $\sim 2\,\mathrm{dB}$ using modest CW pump powers over wavelengths covering the extended telecom bands.

http://dx.doi.org/10.1364/ao.XX.XXXXXX

Four-wave mixing (FWM) has been widely investigated in silicon photonic platforms for use in wavelength conversion, amplification and regeneration of optical data signals [1, 2]. However, there are challenges to increasing the total gain that can be achieved via this process when working in the telecom band owing to the strong two-photon absorption (TPA), and subsequent free carrier generation, that occurs within silicon in this region [3]. Thus, when working with continuous-wave (CW) pump sources required for high repetition rate data signals, integrated p-i-n diodes must typically be employed to reduce the losses associated with build-up of TPA-induced free carriers as the pump powers are increased [4].

An alternative route to increasing the FWM gain is to couple the parametric nonlinear process with the resonant Raman response of the material. This has been successfully demonstrated using silica optical fibers to obtain large gain enhancements for the idler (Stokes beam) when the signal (anti-Stokes) is placed close to the peak Raman shift for the material, even when the FWM process is far from phase-matched [5]. Coupling of the Raman and FWM processes has also been investigated in silicon platforms, but so far the focus has been on conversion via coherent anti-Stokes Raman scattering (CARS) processes, resulting in relatively low conversion efficiencies to the anti-Stokes beam of around $-50\,\mathrm{dB}$ despite the use of high pump powers ($\sim 700\,\mathrm{mW}$) [6]. Additional efforts have looked to exploit CARS conversions in ring-resonator geometries, which have enabled higher conversion efficiencies, exceeding $0\,\mathrm{dB}$, for lower powers ($\sim 20\,\mathrm{mW}$), though with the requirement of higher design complexity and less flexibility in the operating wavelength [7].

In this paper we demonstrate a strong Raman enhancement of FWM wavelength conversion to the Stokes beam in a silicon core fiber (SCF) pumped by a low power CW source in the telecom band. Compared to their planar counterparts, this new class of silicon waveguide combines the benefits of the highly nonlinear core material with the simplicity of the robust and flexible fiber platforms [8]. Specifically, the SCFs used in this work have been tapered using a standard fiber post-processing procedure to control the core size and length, allowing for investigations of the phase-matching conditions on the gain enhancement [9]. The FWM conversion efficiency in the direction of the Stokes wave is found to be orders of magnitude more efficient than for the CARS process, and a maximum conversion efficiency of around $-40\,\mathrm{dB}$ is obtained for a pump power of only $28\,\mathrm{mW}$, when the pump is positioned close to the zero-dispersion wavelength (ZDW) of the tapered SCF. Simulations show that the conversion efficiency can be increased to $\sim 2\,\mathrm{dB}$ for a perfectly phase-matched process with pump powers as low as $\sim 300\,\mathrm{mW}$, providing the first indication that efficient FWM conversion can be achieved in silicon waveguide systems with CW pumping in the telecom band.

The nonlinear processes that contribute to our investigations are depicted in the energy level diagrams of Fig. 1(a), where (1) corresponds to degenerate FWM, (2) is stimulated Raman scattering (SRS), and (3) is inverse Raman scattering (IRS). A schematic of the wavelength conversion processes, highlighting the interaction between them, is also provided in Fig. 1(b). In this image, the pump (ω_p) is launched into the SCF together with the signal (ω_s), which helps to stimulate the FWM process (1). Once FWM induces idler photons (ω_i), SRS can take place as per process (2), which leads to enhancement of the conversion efficiency. However, due to the presence of the FWM enhanced signal, strong IRS conversion can occur, resulting in a transfer of energy back to the pump as per (3). This compensation of the

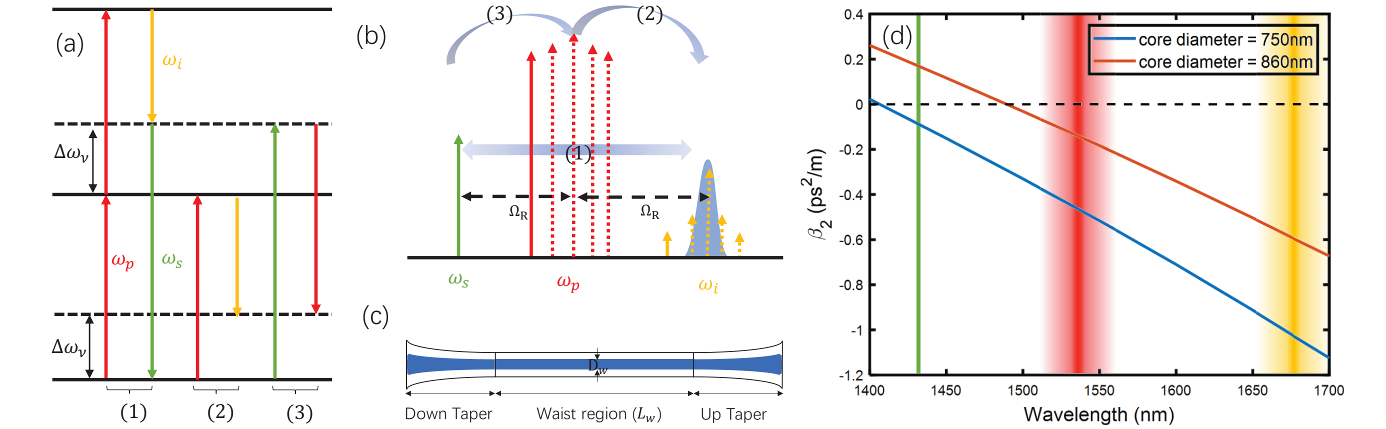

Fig. 1. (a) Energy level diagrams for (1) four-wave mixing, (2) stimulated Raman scattering and (3) inverse Raman scattering. (b) Schematic of frequency conversion occurring due to processes (1-3), as the pump is tuned to align ω_i with the peak Raman gain. (c) Tapered silicon core fiber design. (d) Second-order dispersion parameter as a function of wavelength for SCFs with two different core diameters, as labelled. Vertical lines indicate the positions of the pump (red), signal (green) and idler (yellow).

pump can thus further increase the conversion efficiency of the idler via the FWM (1) and SRS (2) processes. To verify the role of SRS, the pump frequency can be tuned to adjust the alignment of the idler with respect to the peak Raman gain, positioned at Ω_R, as also illustrated in Fig. 1(b). We note that our choice to tune the pump rather than the signal beam was dictated via the availability of suitable laser sources. However, the principal is the same regardless of which beam is tuned, and we expect that when the pump and idler frequencies are separated by the peak Raman shift of the material, the maximum enhancement will take place.

The SCFs used in this work were fabricated via the molten core drawing technique, followed by a subsequent tapering process to tailor the core diameter D_w and length L_w of the waist region [10], shown schematically in Fig. 1(c). The tapering process also helps to improve the crystallinity of the core, which reduces the optical losses, and all SCFs used in this work had low propagation losses of $\sim 2\,\mathrm{dB/cm}$. A portion of the input and output transition regions were retained in the tapered structures to improve the coupling efficiency, thus reducing the insertion loss, though the lengths of these are kept very short ($\sim 1\,\mathrm{mm}$) so that they do not contribute to the nonlinear propagation in the waist. Owing to the phase-matching requirements of FWM, the waist diameter plays a vital role in determining the dispersion properties. To illustrate this, Fig. 1(d) shows second order dispersion (β_2) curves for two SCFs with core diameters of 860 nm and 750 nm, illustrating the blue shifting of the ZDW for smaller cores. The position of the signal wavelength (1431 nm - green), tunable pump (centered at 1545 nm - red) and generated idler (yellow) beams used in our experiments are indicated by the vertical lines. From this it is clear that the pump beam is positioned closer to the ZDW for the SCF with the larger core size, which helps to ensure a broad phase-matching bandwidth.

To model nonlinear propagation in the tapered SCFs, the generalized nonlinear Shrödinger equation (GNLSE) is used as given in the form [11]:

$$\frac{\partial A}{\partial z}+\frac{\alpha}{2}A-i\sum_{n=1}^{\infty}\frac{i^n\beta_n}{n!}\frac{\partial^n A}{\partial t^n}-\frac{\sigma}{2}\left(1+i\mu\right)N_cA=$$
$$i\left(\gamma\left(\omega_0\right)+i\gamma_1\frac{\partial}{\partial t}\right)\left(A(z,t)\int_0^{\infty}R(t')\left|A(z,t-t')\right|^2dt'\right). \quad \textbf{(1)}$$

The terms on the left hand side describe the linear propagation, where A is the pulse amplitude, α is the linear propagation loss, β_n is the nth order dispersive term, and σ is the free carrier parameter for crystalline silicon, with μ and N_c being the free carrier dispersion and density, respectively. The terms on the right hand side govern the nonlinear propagation, where γ is the nonlinearity parameter, $\gamma_1 = \mathrm{d}\gamma/\mathrm{d}\omega \approx \gamma/\omega_0$, and $R(t)$ is the nonlinear response function. For propagation in the telecom band, γ is expressed in terms of the nonlinear refractive index ($n_2 = 5.54\times10^{-18}\,\mathrm{m^2/W}$ at 1545 nm) and two-photon absorption (TPA) coefficient ($\beta_{\mathrm{TPA}} = 10\times10^{-12}\,\mathrm{m/W}$ at 1545 nm) via: $\gamma = k_0n_2/A_{\mathrm{eff}} + i\beta_{\mathrm{TPA}}/2A_{\mathrm{eff}}$, where A_{eff} is the effective mode area ($\sim 0.4\,\mu\mathrm{m}^2$ for a core diameter of 860 nm) [10]. The response function R includes both the electronic and vibrational contributions via [12]:

$$R\left(t\right)=\left(1-f_R\right)\delta\left(t\right)+f_Rh_R(t), \quad \textbf{(2)}$$

where $f_R = g_R\Gamma_R/(n_2k_0\Omega_R)$ represents the fractional contribution of the delayed Raman response in which $g_R = 3.4\times10^{-12}\,\mathrm{m/W}$ is the Raman gain and Γ_R is the gain bandwidth [13]. In silicon, h_R is approximated by the function [12]:

$$h_R\left(t\right)=(\tau_1^{-2}+\tau_2^{-2})\tau_1\exp\left(-t/\tau_2\right)\sin\left(t/\tau_1\right), \quad \textbf{(3)}$$

where $\tau_1 = 10.25\,\mathrm{fs}$ is the photon lifetime and $\tau_2 = 3.03\,\mathrm{ps}$ is the damping time.

The experimental setup to study the interaction between the FWM and Raman processes is shown in Fig. 2. A tunable CW pump laser centered at 1545 nm is combined with a CW signal beam, positioned at the anti-Stokes wavelength of 1431 nm, using a wavelength division multiplexer (WDM), and then coupled into the SCFs using a tapered lens fiber (TLF) with a focal diameter of 2.5 μm and a working distance of 14 μm. Two polarization controllers (PC) were used to adjust the polarization of the pump and signal to optimize the conversion efficiency. The output signals from the SCFs were recorded either via a power meter (PM) or an optical spectrum analyzer (OSA) connected through the optical coupler (OC).

Our investigations begin by studying the interaction of FWM and Raman in a SCF that has a tapered waist diameter $D_w = 860\,\mathrm{nm}$ over a length of $L_w = 10\,\mathrm{mm}$, so that the pump

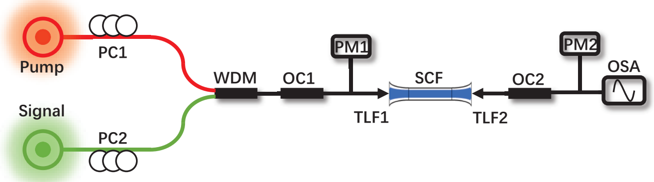

Fig. 2. Experimental setup for Raman enhanced FWM in the tapered SCFs. PC, polarization controller; WDM, wavedivision multiplexer; OC, optical coupler; PM, power meter; TLF, taper lens fiber; OSA, optical spectrum analyzer.

wavelength is close to the ZDW. The experiments were conducted with a pump power of 28 mW and a signal power of only 2 mW. The resulting experimental conversion efficiency is shown as the orange circles in Fig. 3 as the pump wavelength is tuned. As the FWM generated idler wavelength (λ_i) moves closer to the peak Raman wavelength (Λ_R, which is related to the peak frequency Ω_R), the conversion efficiency increases by over an order of magnitude, from ~ -57 dB up to ~ -44 dB, with a clear peak when the offset is zero. To better understand the observed enhancement, the results were compared with simulations of the GNLSE conducted both with (solid curve) and without (dashed curve) the Raman term turned on. As it can be seen, the conversion efficiency for FWM alone is low (~ -55 dB) as the process is not perfectly phase-matched. However, significant enhancements (~ 15 dB) can be achieved when the Raman and FWM processes are coupled, and the simulated results under these conditions are in good agreement with the experiments. To further study the role of phase-matching, additional experiments were conducted for SCFs with different waist diameters: 760 nm (yellow circles) and 750 nm (blue circles), but the same input powers. From these results we see that although the maximum conversion efficiency drops as the FWM moves further from phase-matching for the decreasing core size, significant Raman enhancement can still be achieved, with gains of ~ 12 dB and ~ 9 dB for the 760 nm and 750 nm diameters, respectively. Interestingly, when comparing the simulated FWM conversion efficiencies without Raman, we notice that these curves oscillate. We attribute this behaviour to changes in the phase-matching conditions, and thus the energy transfer between the waves, as the pump is tuned. Due to the phase-mismatch, the energy transfer will also vary as the SCF length is changed, thus we expect that the maximum FWM conversion will depend on L_w.

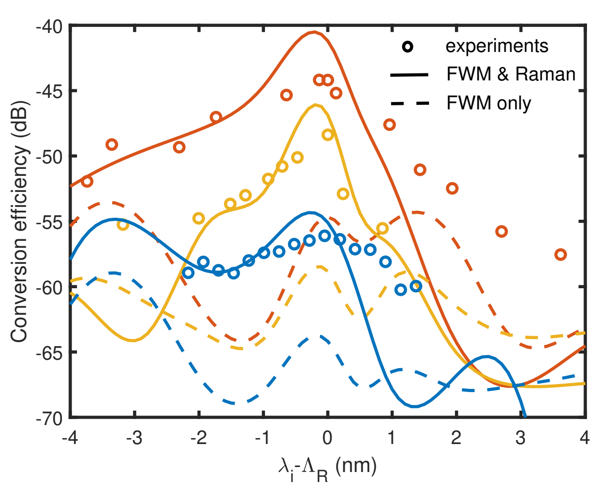

Fig. 3. Conversion efficiency as λ_i is tuned across Λ_R for three different SCF core diameters: 860 nm (orange), 760 nm (yellow) and 750 nm (blue), with $L_w = 10$ mm. Experiments are compared to simulations including FWM & Raman, and with FWM only, as labelled in the legend.

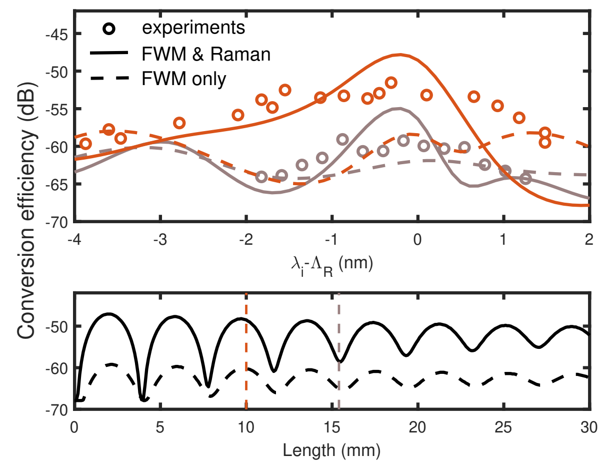

Fig. 4. (a) Comparison of the conversion efficiency as λ_i is tuned across Λ_R for two SCFs with $D_w = 860$ nm, but lengths of $L_w = 10$ mm (orange) and $L_w = 15.4$ mm (grey). Experiments are compared to simulations including FWM & Raman, and with FWM only, as labelled in the legend. (b) Simulated conversion efficiencies as a function of tapered waist length conducted both with (solid) and without Raman (dashed). The vertical lines mark the waist lengths for the SCFs in (a).

To better understand the length dependence of the conversion efficiency, an additional SCF was fabricated with a core waist diameter of 860 nm, but with a longer length of $L_w = 15.4$ mm. Fig. 4(a) plots the measured conversion efficiency as the pump is tuned to position the idler closer to the peak Raman shift Λ_R for the two SCF lengths. For these experiments, the pump power was reduced slightly to 14 mW, but the signal power remained fixed at 2 mW, resulting in a reduced Raman enhancement of ~ 4 dB for the 10 mm fiber (orange circles), as estimated from the simulation results. Although we might expect the Raman gain to increase for increasing fiber length, as the conversion process is initiated by FWM, we find that both the conversion efficiency and enhancement are reduced for the 15.4 mm SCF, by around 7 dB and 4 dB, respectively. This can be understood via plots of the simulated conversion efficiency as a function of length shown in Fig. 4(b), where it is clear that the FWM conversion efficiency varies greatly as the waves move in and out of phase, and that SRS only serves to amplify the conversion rather than alter the trend. From this plot it is clear that the shorter SCF length corresponds to a peak in the FWM conversion, whilst the longer SCF is positioned at a minimum. Importantly, this result also helps us to explain the relatively high conversion efficiency obtained for the 760 nm core diameter SCF compared to the 750 nm SCF in Fig. 3, as the 10 mm length used in these investigations is closer to the optimal length for the larger core fiber.

Although our results have shown that significant enhancements to the FWM wavelength conversion efficiency can be obtained with a phase-mismatch, we expect that much stronger enhancements should be attainable for a system that is perfectly phase-matched, i.e., correct SCF core diameter, pump and signal wavelengths, resulting in more practical output idler powers. Fig. 5 plots simulation results of the conversion efficiency as functions of core diameter and pump wavelength. To compensate for the changing core diameter, the simulations were conducted with fixed pump intensity of 8.6×10^{11} W/m^2, which corresponds to a peak power of 340 mW for a diameter of 860 nm, and signal power of 2 mW. We note that for these simulations higher pump powers were chosen such that they allowed for the maximum conversion efficiency to be achieved, even though TPA and TPA-induced FCA are no longer negligible. In all cases the tapered SCF length was fixed at 10 mm as increasing the length beyond this did not significantly increase the output efficiency. As can be seen, for each SCF core diameter there is an optimum pump wavelength that satisfies the phase-matching conditions, allowing for large conversion efficiencies of up to 2.3 dB, which equates to usable Stokes output powers of several μW for these pump/signal powers. Significantly, these results provide the first indication that FWM conversion efficiencies exceeding 0 dB can be achieved in silicon waveguide systems when pumped in the telecom band with a CW source, without the need for complex p-i-n diode [4] or ring resonator structures [7]. Comparing Fig. 5 to simulations conducted without the Raman term, we find that the gain enhancement due to the nonlinear coupling can reach as high as 28 dB. Moreover, due to the strong coupling to the Raman term, the system is also fairly robust to changes in the pump wavelength and core size, with high conversion efficiencies being maintained over a wavelength band of $\sim$ 20 nm and a $\sim$ 25 nm variation in the diameter. The red shifting of the optimum pump wavelength to allow for phase-matching as the core diameter increases is consistent with the shift in the dispersion profiles seen in Fig. 1(d) [10], and highlights the convenience and flexibility of the tapered SCF platform to cover broad wavelength regions. Furthermore, by fabricating nano-spike couplers onto the SCF facets, these fibers can also be spliced directly into conventional fiber networks, allowing for the construction of robust and practical systems [14].

In summary, this work has demonstrated that by coupling the FWM and Raman terms in low loss tapered SCFs it is possible to achieve a significant enhancement of the conversion efficiency for CW pump beams with fairly modest power levels. Our experiments have shown that the maximum conversion efficiency depends on the phase-matching conditions and length of the tapered waist, but that substantial enhancements up to $\sim$ 15 dB can be obtained even under non-phase-matched conditions. By tailoring the core size to optimize the phase-matching, our simulations have shown that it should be possible to obtain large FWM conversion efficiencies of the order of a few dB without the need for complex carrier sweep-out schemes [4], or the use of pulsed pumps [2]. These results highlight the power of exploiting coupling between the parametric and resonant nonlinear processes for boosting the output signal powers from practical systems.

Acknowledgments. The authors would like to thank EPSRC (EP/P000940/1), NSFC (Grant N0.62175080), J. E. Sirrine Foundation and the CSC for funding of the project, and Dr S. Liang for use of their equipment. The data that support the findings of this study are openly available in the University of Southampton Institutional Research Repository.

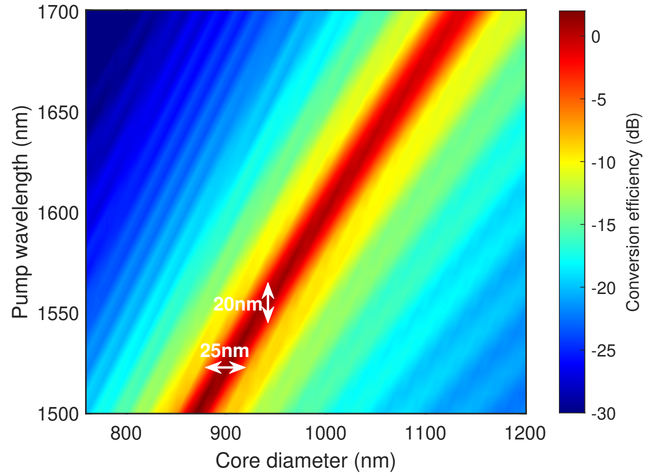

Fig. 5. Simulated conversion efficiency as functions of the tapered SCF core diameter and pump wavelength, for a fixed length of 10 mm. The input pump intensity is set as 8.6×10^{11} W/m^2, with a signal power of 2 mW.

REFERENCES

1. R. L. Espinola, J. I. Dadap, R. M. Osgood, S. J. McNab, and Y. A. Vlasov, Opt. Express **13**, 4341 (2005).
2. M. A. Foster, A. C. Turner, J. E. Sharping, B. S. Schmidt, M. Lipson, and A. L. Gaeta, Nature **441**, 960 (2006).
3. P. Kanakis, T. Kamalakis, and T. Sphicopoulos, J. Opt. Soc. Am B **31**, 366 (2014).
4. A. Gajda, L. Zimmermann, M. Jazayerifar, G. Winzer, H. Tian, R. Elschner, T. Richter, C. Schubert, B. Tillack, and K. Petermann, Opt. Express **20**, 13100 (2012).
5. T. Sylvestre, H. Maillotte, E. Lantz, and P. T. Dinda, Opt. Lett. **24**, 1561 (1999).
6. R. Claps, V. Raghunathan, D. Dimitropoulos, and B. Jalali, Opt. Express **11**, 2862 (2003).
7. N. Vermeulen, J. Sipe, and H. Thienpont, IEEE Photonics Technol. Lett. **22**, 1796 (2010).
8. A. C. Peacock, U. J. Gibson, and J. Ballato, Adv. Physics: X **1**, 114 (2016).
9. D. Wu, L. Shen, H. Ren, J. Campling, T. W. Hawkins, J. Ballato, U. J. Gibson, and A. C. Peacock, APL Photon. **4**, 086102 (2019).
10. D. Wu, L. Shen, H. Ren, M. Huang, C. Lacava, J. Campling, S. Sun, T. W. Hawkins, U. J. Gibson, P. Petropoulos, J. Ballato, and A. C. Peacock, IEEE J. Sel. Top. Quantum Electron. **27**, 1 (2020).
11. L. Yin, Q. Lin, and G. P. Agrawal, Opt. Lett. **31**, 1295 (2006).
12. G. P. Agrawal, "Nonlinear fiber optics," in *Nonlinear Science at the Dawn of the 21st Century*, (Springer, 2000), pp. 195–211.
13. M. Huang, S. Sun, D. Wu, H. Ren, L. Shen, T. W. Hawkins, J. Ballato, U. J. Gibson, and A. C. Peacock, APL Photon. **6**, 096105 (2021).
14. H. Ren, O. Aktas, Y. Franz, A. F. J. Runge, T. Hawkins, J. Ballato, U. J. Gibson, and A. C. Peacock, Opt. Express **25**, 24157 (2017).